The Role of Wheel Alignment Over the Fatigue Damage Accumulation in Vehicle Steering Knuckle

K. Reza Kashyzadeh[a] , G.H. Farrahi[b,*] , M. Shariyat[c] , M.T. Ahmadian[b]

[a]School of Science and Engineering, Sharif University of Technology, International Campus, Kish Island, Iran.
[b]School of Mechanical Engineering, Sharif University of Technology, Tehran, Iran.
[c]Faculty of Mechanical Engineering, K.N. Toosi University of Technology, Tehran, Iran.

Article info

Abstract

The present paper investigates the effect of changes in wheel primary angles such as Camber and Toe angles on the fatigue life of vehicle steering knuckle under multi-input random non-proportional 3D stress components. In order to develop real loading conditions for the steering knuckle, the localizing equivalent road as a combination of some rough roads (ISO road classification B-F for highway out of town, urban highway, urban asphalt, soil road, and flagstone, respectively) based on statistical data collected from different cities by utilizing a general questionnaire including road type and vehicle velocity was considered. Then, the various actual load histories obtained through multi-body dynamics analysis of a full vehicle model were applied on several points of the component. The fatigue life of steering knuckle was predicted by using some prominent multi-axial fatigue criteria for non-proportional loading, rain-flow cycle counting algorithm, and Palmgren-Miner damage accumulation rule. Finally, the effect of different values of wheel angles on the fatigue life of the steering knuckle was examined. The results showed that the highest and lowest fatigue life of steering knuckle are related to the values of 2 positive and negative degrees of camber angle, respectively. The stress level is reduced in the various equivalent load histories by changing the toe angle to 0.2 negative, resulting in an increase in the fatigue life of steering knuckle.

Nomenclature

R_{eq}	Equivalent road	t	Time
X	Road length	θ, φ, ϕ	Eulerian angles
α_i	Share of various ISO road classification in percentage	$\tau_{af,R=-1}$	Shear fatigue strength under fully reversed loading
$a, b, c, d,$ f, k, α, β	Material-dependent parameters	$\sigma_{af,R=-1}$	Tension-compression fatigue strength under fully reversed loading
J_2	Second deviatoric stress invariant	N_f	Number of cycles to failure
K	Shear yield stress of the material	N_O	Reference number of loading cycles (2×10^6)
S_i	Principle stress components	σ_{eq}	Equivalent stress
σ_{ij}	Stress tensor components	σ_u	Ultimate stress of the material

σ_f	Tensile yield stress of the material	σ_m	Mean stress
σ_n	Normal stress acting on a plane	σ^H	Hydrostatic stress
τ_a	Amplitude of shear stress acting on a plane	$\sigma_{\max}^H$	Maximum mean hydrostatic stress
$N_{a,eq}$	Equivalent uniaxial normal stress	N_m	Mean normal stress

1. Introduction

One of the most safety critical components of the vehicle which is affected by different loads is the steering knuckle. Establishing the connection between drive shaft, steering system, wheel, suspension system, and car chassis is the main task of this part. Therefore, if this piece breaks down, it causes problems in handling and controlling the vehicle. This may lead to irreparable accidents.

This component does not have a particular shape and design. Hence, it can be seen with different capacities and materials in various types of vehicles. In addition, the particular positioning of the steering knuckle in the vehicle and maintaining its initial position during various maneuvers can have a significant effect on the loads that are exerted on several points of the component. The steering knuckle location is generally examined by two parameters:

1. Reference points, which must be compatible with one another in order to be connected to other vehicle components such as the location of the wheel hub.

2. Wheel angles, recommended by the manufacturer for the stability of the vehicle.

There are several signs to identify the changes occurring in wheel angles. One of the most famous indications of these is tire-erosion. Reduced handling is another one of the hallmarks of this issue. In other words, steering wheel must not deviate to the left or right while driving, even if it is released.

There are several reasons for changing the initial wheel angles settings; most notably may refer to the following:

1. High-speed driving on low-quality roads such as soil and flagstone roads removes wheel angles from their initial balance settings.

2. Lack of care in exactly configuring wheel angles by car repairers.

In order to study of the effect of wheel angles on the vehicle behaviors including handling, controlling, stability and dynamic performance, it is necessary to simulate road roughness as the main sources of shocks exerted on the vehicle components. Therefore, many researchers have tried to identify, measure, and classify it by using different methods.

Sayers et al. have introduced two common methods for measurement of road roughness. One method uses the topographic camera that records ups and downs of the road directly, and the other uses strain gauges being installed to a vehicle under test operation [1-2]. Then, some road roughness profiles have been recorded for the federal highway organization by using profiler [3]. Gonzalez has presented a new approach to obtain road roughness by utilizing accelerometers. The calibration formulas were derived to estimate different types of road roughness by using accelerometer data [4]. Johnson et al. have proposed a time-independent Laplace model to measure road roughness. The model covers both standards of ISO and IRI [5]. In recent years, mobile laser scanning [6] and sensor network of smartphones [7] are used for road roughness detection and monitoring. Choi et al. have used 3D scanning method for obtaining road surface. They focused that the road profile can be changed by erosion and vehicle movements. Thusly, in order to have the accurate vehicle tests, it is important to reproduce and repair the road surface [8].

In the last decade, the effect of vehicle velocity on the vehicle dynamic response due to road roughness has been studied. Kashyzadeh et al. have reported wide and narrow band random vibration for low (34Km/h) and high (100Km/h) speed of passenger car, respectively. Another research reported white noise for both of low and high speed of heavy vehicles [9]. Barbosa has investigated the vertical and angular modal vehicle dynamic response due to pavement roughness by using PSD function. A huge movement amplification for the first mode of vibration at high speed (120Km/h) has been reported which can damage passenger [10]. The effect of speed on road roughness sensing and pavement performance reduction has also been studied [11-12].

During service time of a vehicle, various multiaxial variable amplitude loadings are exerted on the vehicle body and components. These loading conditions depend on various parameters such as driving on road roughness, vehicle speed, driver's behavior, vehicle settings, etc. The nature of these loads is cyclic and can cause fatigue phenomena in vehicle components. Thus, it is necessary to extract the real time history of forces on different critical components by using road roughness simulations and multi-body dynamics analysis of a full vehicle model. After that, fatigue analysis should be performed to predict safe servicing time period of all critical components and they can be replaced before they fail. To this end, a few studies have been done in the field of failure of steering knuckle as a highly critical component.

Fracture characteristics of fatigue failure of auto-

motive steering knuckle made of ductile iron have been investigated. For this purpose, a thick slice was cut off near the fracture part in order to take chemical analysis by Optical Emission Spectroscopy (OES) and optical metallography. The Charpy V-notch impact test were performed and the Scanning Electron Microscope (SEM) images were used to topography analysis. Finally, fatigue phenomenon was presented as the main reason of this failure [13]. Sivananth et al. have calculated fatigue life of steering knuckle made of SG iron and aluminum alloy based on stress-life approach [14]. Azrulhisham et al. have evaluated fatigue life reliability of steering knuckle by utilizing Pearson parametric distribution model [15]. Vivekananda et al. have estimated fatigue life of aluminum alloy steering knuckle by using mathematical calculation, applying S-N curve, and different mean stress theories (Goodman, Gerber, and Soderberg) [16]. Bhokare et al. have predicted fatigue life of the knuckle arm of a sport vehicle [17]. Farrahi et al. have investigated fatigue damage of the rear spindle of the vehicle [18]. Shariyat has developed random fatigue model by modification of Gough's theory [19]. He has presented a new energy-based equivalent stress criteria for fatigue life determination in components with complicated geometry under random non-proportional 3D stress fields [20-21]. Fatemi et al. have studied the effect of various parameters of the production process on the fatigue life of steering knuckle made of forged steel by using experimental [22] and analytical [23] methods. Zoroufi et al. have studied the experimental durability assessment and life prediction of steering knuckles made of different materials including forged steel, cast iron, and aluminum alloy [24].

Recently, physical parameters of the tire have attracted the attention of automotive laboratories and research centers because of the role of the tire as the interface between road roughness and vehicle parts. The effect of the tire size on the fatigue damage of vehicle bodies has been studied by Schon [25] and Angelo [26]. The results showed that the standard tire size, suggested by the automobile manufacturer, caused the least fatigue damage, and increasing tire size led the fatigue damage to increase at the critical points of the vehicle body.

The previous researchers analyzed fatigue life of knuckle under axial constant amplitude loading or proportional multi-axial loading (sinusoidal wave with same phases), and non-proportional multi-axial loading (sinusoidal wave with varying phases) conditions by utilizing Belgian road data. But, in the present paper, the fatigue life of steering knuckle is predicted by using some prominent multi-axial fatigue criteria for non-proportional loading. To achieve this purpose, the equivalent road model is provided using statistical data collected from different cities. Subsequently, the most

critical loading conditions for steering knuckle are obtained through multi-body dynamics analysis of a full vehicle model during driving on the equivalent road using driving control based on non-constant speed. For the first time, the effect of two wheel alignment angles including Toe and Camber, on the fatigue life of automotive steering knuckle is investigated.

2. Vehicle Driving Simulation

The virtual durability testing is generally specified in three steps, including load history prediction, stress/strain analysis, and fatigue life assessments. In order to perform fatigue assessments, the experienced stress or strain distribution from loading should be known. In this section, the various actual load histories exerted on several points of the component were obtained through multi-body dynamics analysis of a full vehicle model. The force histories extraction process methodology used in this paper is shown in Fig. 1 and each step will be described in the following sections.

2.1. Equivalent Road Profile

A vehicle passes over roads having different surface qualities during its lifetime. Each road causes a certain fatigue damage on automotive components due to the vehicle velocity and various maneuvers such as acceleration, braking, etc. Because the quality of roads in different parts of a country, city, or even street is not the same throughout, the best and most accurate way to get the unevenness of a road surface is to obtain an equivalent road profile to estimate loading histories of automotive components..

The International Organization for Standardization (ISO) has proposed a classification of road roughness (A-H) based on spectral density function. Time history of various types of road roughness can be obtained by using Inverse Fast Fourier Transform (IFFT) [27]. In this research, a combination of different types of roughness (ISO road classification B-F for highway out of town, urban highway, urban asphalt, soil road, and flagstone, respectively) is used based on statistical data collected from Iranian car drivers in several cities by utilizing a general questionnaire including road type and vehicle velocity. This combination and its corresponding vehicle velocity are indicated in Fig. 2 and Fig. 3, respectively.

The equivalent road is also considered as follows:

$$R_{eq} = (\alpha_{\text{stright}} + \alpha_{\text{breaking}} + \alpha_{\text{acceleration}} + \alpha_{\text{cornering}})X \quad (1)$$

Where X is the road length, R_e and α_i are the equivalent road and the share of various ISO road classifications in percentage, respectively.
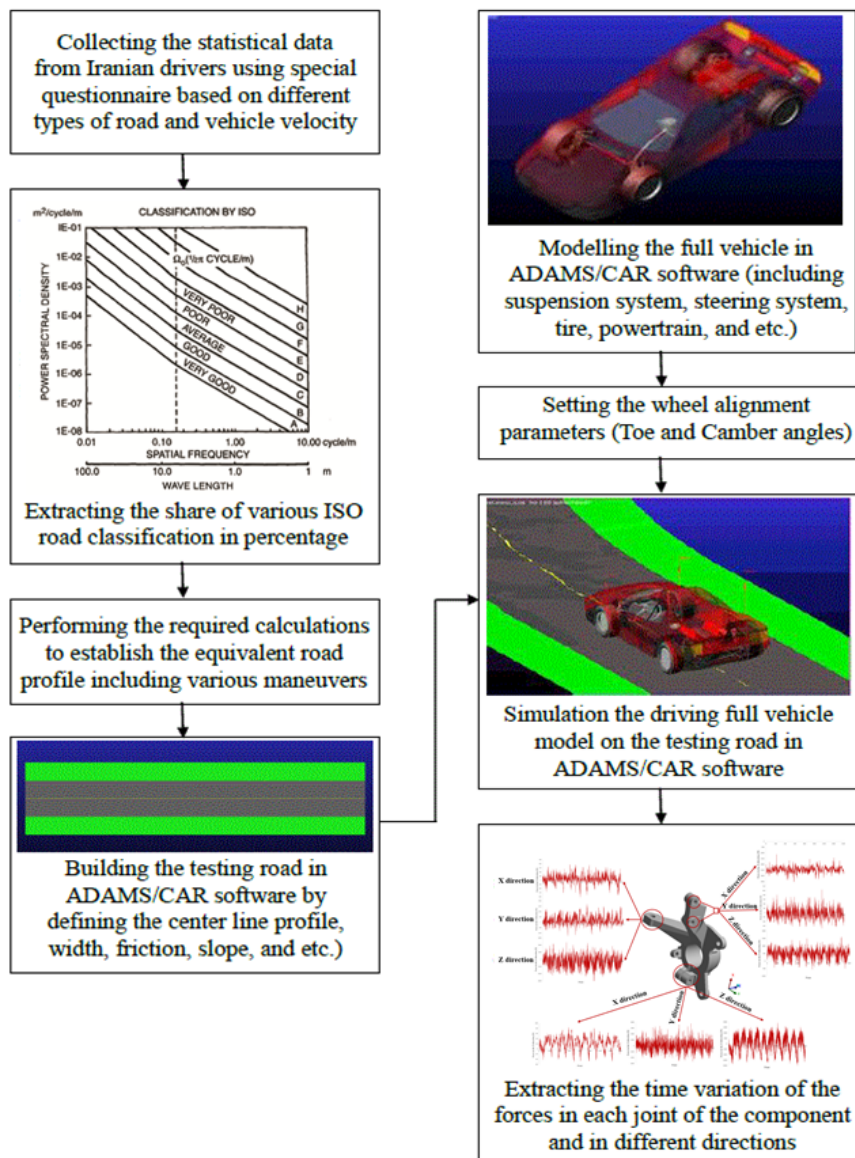
Fig. 1. Flowchart of the force histories extraction process.

In this research, braking and acceleration maneuvers have been neglected since their effects on the fatigue damage of automotive components are not significant in comparison with the effects of straight driving [18]. The test road consists of 95% straight driving effects and 5% cornering effects. For straight driving, the following five maneuvers have been considered:

- 102.34km/h on road type B ($\alpha_B = 30.3\%$)

- 66.7km/h on road type C ($\alpha_C = 40.4\%$)

- 36.2km/h on road type D ($\alpha_D = 20.6\%$)

- 18.5km/h on road type E ($\alpha_E = 7.1\%$)

- 4km/h on road type F ($\alpha_F = 1.6\%$)

The fast cornering has been considered for studying cornering effects [18, 28] as it causes more damage compared to slow or moderate cornering.

Fast cornering with constant radius 30 meters (50km/h on road type C)
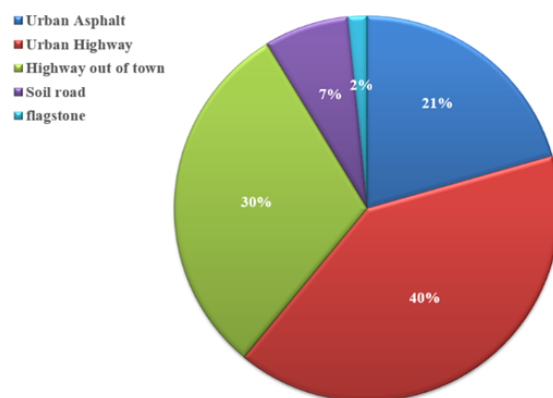
Fig. 2. Combination of different roads for passenger cars.
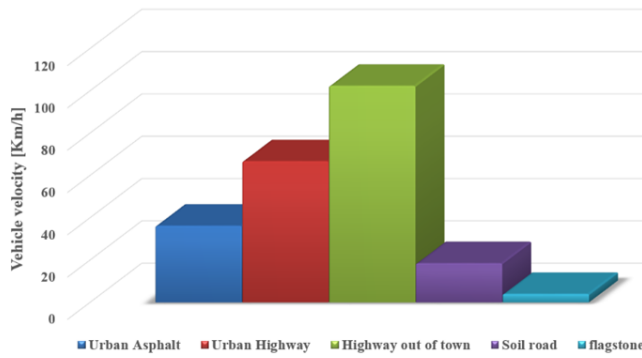
Fig. 3. Vehicle velocity for various roads.

2.2. Details of Full Vehicle Model

The driving full-vehicle model has been simulated in Adams software. A four cylindrical passenger car with a 1500cc and 78hp power engine as well as a 1013kg kerb weight and 1670kg gross weight is simulated. This model consists of several main sub-models such as MacPherson front suspension system, twist beam for rear suspension system, rack and pinion types of steering system, front and rear wheels, body, etc.

The distance between the two lateral axes is 1455mm, and the distance between the rear and front axles is 2415mm. The front spring stiffness isconsidered to have a non-linear behavior as shown in Fig. 4. The damper coefficient for the right and left sides

areconsidered as 3105 and 1368N.s/m, respectively.
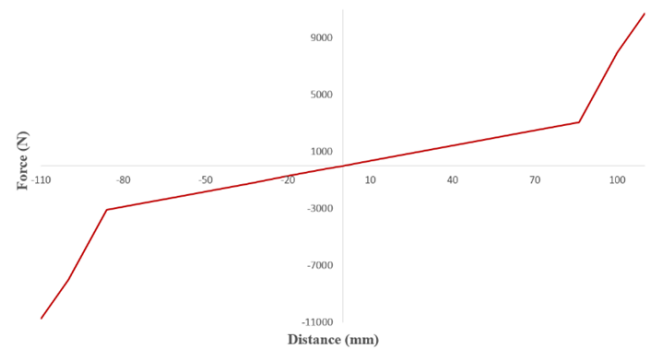
Fig. 4. Diagram of spring behavior.

The tires are modeled as 175/70/R13 for the present research. The physical properties of the tire are reported in Table 1. Toe and Camber angles are considered as -0.1 and 2 degrees based on the recommendation of the manufacturer. The full vehicle model in Adams is illustrated in Fig. 5.

2.3. Loads and Details of the Component

Steering knuckle is a critical component of the vehicle. It is made up of cast iron with an ultimate tensile strength of 480MPa (Fig. 6).

Force histories have been extracted in three different points of steering knuckle including the joint of the

Table 1
Physical properties of tire 175/70/R13.

Parameter	Radius	Width	Wall	Mass	Area	Volume
Unit	mm	mm	mm	Kg	Square meter	Cubic meter
Value	165.1	175	122.5	22.218	1.173	0.033
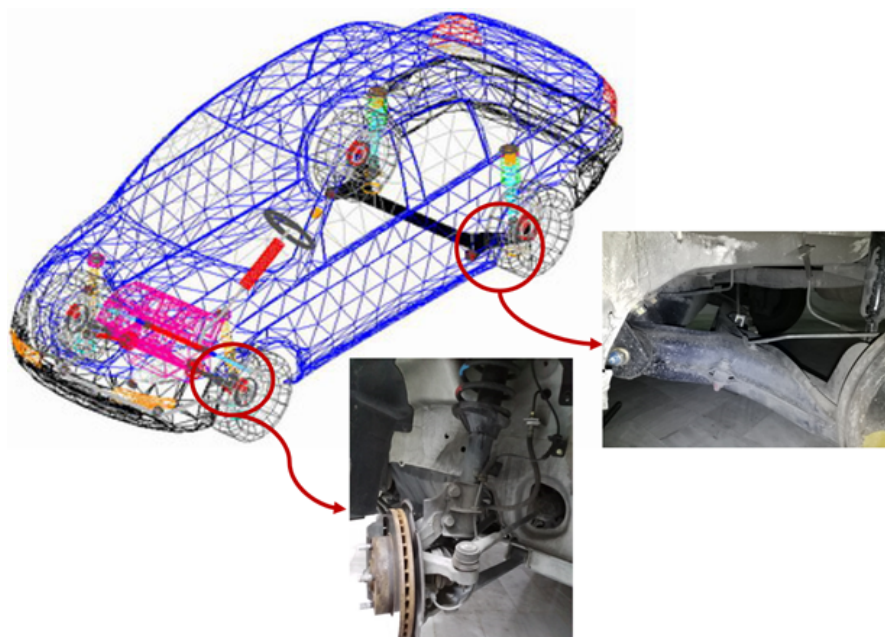
Fig. 5. Full-vehicle model in Adams Software.

Table 2

Statistical data of loading histories for Toe angles.

Points of application	Toe angle	Mean load (N)					Min. load (N)					Max. load (N)				
		+0.2	+0.1	0	-0.1	-0.2	+0.2	+0.1	0	-0.1	-0.2	+0.2	+0.1	0	-0.1	-0.2
Joint of the	X	320	783	1030	1025	1100	-2094	-368	-333	-352	-345	-51	42	15	17	92
knuckle and the	Y	809	399	414	422	420	-160	-719	-962	-944	-1017	59	-49	-4	-2	-61
steering linkage	Z	1117	2033	2789	2776	2970	-131	-3921	-3845	-3907	-3869	-303	-233	-77	-116	-81
Joint of	X	11333	17861	18302	16879	18180	-379	-798	-1082	-1187	-885	3488	4586	3317	3172	4288
lower	Y	1535	1640	1653	1655	1651	-1534	-3681	-3748	-3738	-3736	141	-257	200	184	-173
control arm	Z	1942	7241	6246	4274	6356	-2244	-12055	-12261	-10690	-12081	110	-295	296	565	338
Joints of the	X	-248	572	995	555	551	-13877	-15200	-15499	-5753	-6593	-15415	-6017	-5794	-2398	-6186
knuckle and	Y	572	2901	2941	2923	2903	-487	-429	-441	433	-420	-145	402	-119	-104	258
MacPherson strut	Z	1394	1506	1508	1510	1515	20	-43	-84	-76	-57	588	612	585	601	630

Table 3

Statistical data of loading histories for Camber angles.

Points of application	Camber angle	Mean load (N)					Min. load (N)					Max. load (N)				
		+2	+1	0	-1	-2	+2	+1	0	-1	-2	+2	+1	0	-1	-2
Joint of the	X	1025	630	584	418	420	-352	-369	-655	-933	-1301	17	-17	-15	-32	-28
knuckle and the	Y	422	452	529	807	1062	-944	-741	-547	-396	-302	-2	21	24	35	46
steering linkage	Z	2776	2222	2288	1911	1590	-3907	-3887	-4322	-4635	-4750	-116	-156	-169	-259	-254
Joint of	X	16879	17878	17259	16745	16330	-1187	-1027	-1030	-939	-915	3172	3614	3548	3205	3232
lower	Y	1655	1684	683	1657	1669	-3738	-3669	-3516	-3428	184	196	-528	211	287	
control arm	Z	4274	6142	6512	6490	5863	-10690	-13186	-13555	-13904	-565	340	105	42	1	
Joints of the	X	555	482	913	878	909	-6593	-7753	-15498	-15521	-15487	-2398	-2843	-5740	-5692	-5771
knuckle and	Y	2923	2695	2916	2928	2899	-433	-445	-452	-451	-435	-104	-135	-128	-125	-200
MacPherson strut	Z	1510	1508	1504	1499	1400	-76	-83	-84	-62	-77	601	572	571	587	576

knuckle and the steering linkage, joint of the lower control arm, and joints of the knuckle and MacPherson strut. These loading conditions are demonstrated in Fig. 7. The wheel hub is considered to be fixed in all degrees of freedom (DOF).

Below, different loading histories for various values of Toe and Camber angles are obtained. Statistical data of obtained conditions versus angle changes are reported in Tables 2 and 3.

Fig. 6. Front steering knuckle in driver's side of a four cylindrical passenger car.
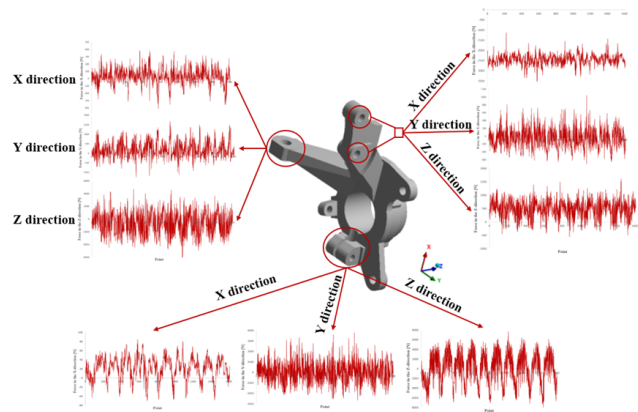
Fig. 7. Loading conditions for different points of the steering knuckle.

3. Fatigue Assessment

The transient stress analysis was performed to determine the critical points of failure for the steering knuckle. The finite element results indicated that the joint of the knuckle and the steering linkage is the most critical region (see Fig. 8).

Time histories of 3D stress components were extracted for critical elements. Then, equivalent stress was calculated by using different criteria for multi-axial non-proportional loadings. The considered fatigue criteria are presented in the following sub-sections.
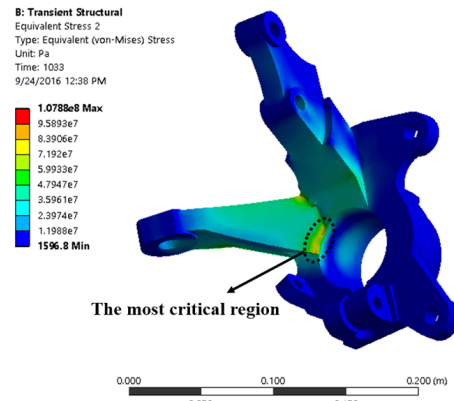
Fig. 8. Distribution of Von-Misses stress for steering knuckle and determining critical region.

3.1. Brief Overview of the Theoretical Foundations of the Considered Fatigue Theories

The conventional strategies for fatigue life prediction are based on axial stress state. But, these criteria are not appropriate for fatigue life determination in the large industrial components with complicated geometries under multi-input loading conditions. Hence, many stress-based multiaxial fatigue failure criteria have already been developed based on experimental observations. Multiaxial criteria are used to calculate an equivalent uniaxial stress state from a stress tensor

and enable the use of cycle counting methods. Some of these criteria, as well as some recently proposed criteria, are presented in this study.

3.1.1. Von-Misses Criterion

Von-Misses criterion may be expressed as:

$$J_2 = K^2 \tag{2}$$

Where J_2 and k are the second deviatoric stress invariant and the shear yield stress of the material, respectively. For a 3D stress field, one may write:

$$
\begin{aligned}
J_2 &= \frac{1}{2}s_{ij}s_{ji} = \frac{1}{2}tr(s^2) = \frac{1}{2}(s_1^2 + s_2^2 + s_3^2) \\
J_2 &= \frac{1}{2}s_{ij}s_{ji} = \frac{1}{2}tr(s^2) = \frac{1}{2}(s_1^2 + s_2^2 + s_3^2)
\end{aligned} \tag{3}
$$

$$
\begin{aligned}
J_2 = \frac{1}{6}[&(\sigma_{11} - \sigma_{22})^2 + (\sigma_{22} - \sigma_{33})^2 \\
&+ (\sigma_{33} - \sigma_{11})^2] + [(\sigma_{12})^2 + (\sigma_{23})^2 + (\sigma_{31})^2]
\end{aligned} \tag{4}
$$

and

$$K = \frac{\sigma_f}{\sqrt{3}} \tag{5}$$

where σ_f is the uniaxial tensile yield stress of the material.

3.1.2. Findley Criterion

Findley has proposed that fatigue failure occurs when the superposed magnitudes of the normal stress and fluctuation amplitude of the shear stress acting on a plane, become equal to $\tau_{af,R=-1}$. Its original form is [29]:

$$(\tau_a + K\sigma_n)_{\max(\theta,\varphi,\phi)} = f \tag{6}$$

The Findley constants, K and f are defined as [29]:

$$K = \frac{2 - (\sigma_{R=-1}/\tau_{R=-1})}{\sqrt[2]{(\sigma_{R=-1}/\tau_{R=-1}) - 1]}} \tag{7}$$

$$f = \sqrt{\frac{(\sigma_{R=-1})^2}{4[(\sigma_{R=-1}/\tau_{R=-1}) - 1]}} \tag{8}$$

By substituting the defining constants as above and simplifying the Findley criterion, it will be as follows:

$$\sigma_{eq} = \sqrt{\begin{array}{c}(4\Sigma - 4)C_a^2 + (2 - \Sigma)^2 N_{\max}^2 \\ + \frac{(4\Sigma - 4)(2 - \Sigma)}{\sqrt{\Sigma - 1}}C_a N_{\max}\end{array}} \tag{9}$$

The critical plane is defined as the $\max_{\theta,\varphi,\phi,t}(\tau_a + K\sigma_n)$, where θ, φ, and ϕ are the Eulerian angles and t denotes the time.

    A modified Findley's criterion has been presented by Shariyat [19]. This new approach has shown better results in comparison with the experimental data for the anti-roll bar of a passenger car. The new form of this criterion is expressed as [19]:

$$\tau_{eq} = \max_{\theta,\varphi,\phi,t} \frac{\tau_a + k\sigma_n}{\sqrt{1 + k^2}} \frac{\tau_{af,R=-1}}{\tau_{af,R}} = \tau_{af,R} \tag{10}$$

3.1.3. MacDiarmid Criterion

According to the MacDiarmid Fatigue Criterion, the critical plane is a plane wherein the maximum shear stress amplitude occurs. The original form of this criterion can be expressed as follows [29]:

$$\tau_a + K(\sigma_n)_{\max \tau(t)} = f \tag{11}$$

The MacDiarmid constants, K and f are defined as [29]:

$$K = \frac{(\tau_f)_{A \text{ or } B}}{2\sigma_u} \tag{12}$$

$$f = (\tau_f)_{A \text{ or } B} \tag{13}$$

where σ_u is the ultimate strength of the material and A or B subscripts denote the surface or depth crack propagation concepts introduced by Brown and Miller. This criterion can be rewritten by substituting original model with the defined constants:

$$\tau_{eq} = \frac{2\sigma_u \tau_a}{2\Sigma\sigma_u - (\sigma_n)_{\max \tau(t)}} \tag{14}$$

Recently, Shariyat has proposed a modification form of this criterion that is more accurate than original form when order of the normal stress is much higher than of the shear stress [19]:

$$\tau_{eq} = \left[\tau_a + \frac{\sqrt{1 + K^2}}{K}(\sigma_n)_{\max \tau(t)}\right] \cdot \frac{\tau_{af,R=-1}}{\tau_{af,R}} \tag{15}$$

And

$$K = \frac{2\tau_{af,R} - \sigma_{af,R}}{\sigma_m + \sigma_{af,R}} \tag{16}$$

where σ_m is the mean stress.

3.1.4. Dang Van Criterion

Dang Van has presented a new approach based on Sines idea and applying hydrostatic stress (σ^H). The effect of hydrostatic stress has been included into the equivalent stress definition [29]. According to this criterion, a plane on which the following expression holds first is a critical plane.

$$\tau_a + \alpha\sigma_{\max}^H = \tau_{R=-1} \tag{17}$$

where $\sigma_{\max}^H$ is the maximum mean hydrostatic stress and the parameters α and Σ are defined as [29]:

$$\alpha = 3\left(\Sigma^{-1} - \frac{1}{2}\right) \tag{18}$$

$$\Sigma = \frac{\sigma_R = -1}{\tau_{R=-1}} \tag{19}$$

3.1.5. Carpinteri-Spagnoli (C-S) Criterion

Carpinteri and Spagnoli (C-S) have proposed a new fatigue criterion that was originally an extension of von Misses criterion (for a 2D stress field with one tensile and one shear stress components). It can transform the multiaxial non-proportional stresses into an equivalent uniaxial normal stress which can be written as follows [30, 31]:

$$\sigma_{a,eq} = \sqrt{N_{a,eq}^2 + \left(\frac{\sigma_{af,R=-1}}{\tau_{af,R=-1}}\right)^2 C_a^2} = \sigma_{af,R=-1} \quad (20)$$

$$N_{a,eq} = N_a + \sigma_{af,-1}\left(\frac{N_m}{\sigma_u}\right) \quad (21)$$

where N_m and N_a are the mean and amplitude normal stress, respectively ($N_{\max} = N_m + N_a$). And C_a is the amplitude of shear stress. The $\sigma_{af,R=-1}$ and $\tau_{af,R=-1}$ are the tension-compression and shear fatigue limits which can be determined by using Basquin-type relations [32]:

$$\sigma'_{af,R=-1} = \sigma_{af,R=-1}\left(\frac{N_f}{N_0}\right)^m \quad (22)$$

And

$$\tau'_{af,R=-1} = \tau_{af,R=-1}\left(\frac{N_f}{N_0}\right)^{m^*} \quad (23)$$

where $\sigma'_{af,R=-1}$ and $\tau'_{af,R=-1}$ are the fatigue strength for fully reversed normal and shear stresses at finite life (N_f), respectively. And N_0 is the reference number of loading cycles, e.g. 2×10^6 for both cases. Recently, the effects of critical plane orientation on the multiaxial high cycle fatigue assessment have been studied and the modification form of C-S criterion has been presented [31].

3.1.6. Liu-Zenner Criterion

Liu-Zener criterion considers and distinguishes between effects of the tensile and compressive mean stresses and is calibrated based on the 1D fatigue strengths considering the actual R ratio [19]:

$$\sigma_{a,eq} = \sqrt{a\tau_a^2 + b\sigma_a^2 + c\tau_m^2 + d\sigma_m^2} = \sigma_{af,R=-1} \quad (24)$$

where [19]:

$$a = \frac{1}{5}\{3\Sigma^2 - 4\} \quad (25)$$

$$b = \frac{2}{5}\{3 - \Sigma^2\} \quad (26)$$

$$c = \frac{7}{4}\left\{\left(\frac{2\sigma_{af,R=-1}}{\tau_{af,R=0}}\right) - \Sigma^2\right\} \quad (27)$$

$$d = \frac{7}{5}\left\{2\Sigma\sigma_{af,R=-1} - \frac{\sigma_{af,R=0}}{2}\left(1 + \frac{4c}{21}\right)\right\} \quad (28)$$

3.1.7. Shariyat Criterion

Shariyat has presented some new criteria to assess the equivalent stress adequate for non-proportional random loadings. The validation of these new criteria has been done by comparison with the experimental results for an anti-roll bar of a commercial vehicle. He has proposed a new form of the equivalent stress by using fatigue strength values which can be determined using S-N-P and T-N-P diagrams incorporating the effect of mean stress. This criterion can be described as [19-21]:

$$\frac{[\sigma(t)]_{eq}}{(\sigma_{\max})R} = \left\{\frac{1}{2}\left(\left[\frac{\sigma_x(t)}{(\sigma_{\max})Rx} - \frac{\sigma_y(t)}{(\sigma_{\max})Ry}\right]^2\right.\right.$$

$$+ \left[\frac{\sigma_y(t)}{(\sigma_{\max})Ry} - \frac{\sigma_z(t)}{(\sigma_{\max})Rz}\right]^2 + \left[\frac{\sigma_z(t)}{(\sigma_{\max})Rz} - \frac{\sigma_x(t)}{(\sigma_{\max})Rx}\right]^2$$

$$+ 2\left(\left[\frac{\tau_{xy}(t)}{(\tau_{\max})Rxy}\right]^2 + \left[\frac{\tau_{xz}(t)}{(\tau_{\max})Rxz}\right]^2\right.$$

$$\left.\left.+ \left[\frac{\tau_{yz}(t)}{(\tau_{\max})Ryz}\right]^2\right)\right)\right\}^{\frac{1}{2}} \quad (29)$$

where:

$$(\sigma_{\max})_{Rij} = (\sigma_m)_{ij} +$$

$$(\sigma_{f,R=-1})_{ij}\left(\frac{N_{\sigma ij}}{N_0}\right)^b\left[1 - \frac{(\sigma_m)_{ij}}{\sigma_u}\right], \quad i,j = x,y,z \quad (30)$$

Recently, he has proposed new Energy and Integral approaches which have complex calculations [20, 21]. In the proposed energy-based approach, the effect of hydrostatic stress has been considered as sign function on the fatigue failure. It can be expressed as [20]:

$$\sigma_{eq}(t) = \alpha\sqrt{\begin{array}{c}(\sigma_x(t) - \sigma_y(t))^2 + (\sigma_y(t) - \sigma_z(t))^2 \\ + (\sigma_z(t) - \sigma_x(t))^2 \\ + 6((\tau_{xy})^2 + (\tau_{xz})^2 + (\tau_{yz})^2)\end{array}} \quad (31)$$

$$+ \beta\sigma_h(t)$$

where

$$\alpha = \frac{\sqrt{2}}{2} \quad (32)$$

$$\beta = 3\left(\sqrt{3}\Sigma\frac{\left(1 - \frac{\sigma_m}{\sigma_u}\right)}{\left(1 - \frac{\tau_m}{\tau_u}\right)} - 1\right) \quad (33)$$

And the form of Shariyat's integral approach may be described as follows [21]:

$$\sigma_{a,eq} = \frac{1-R}{2\left(1 - \dfrac{\sigma_{eq,m}}{\sigma_u}\right)} \times \sqrt{\frac{3}{8\pi}\int_{\theta=0}^{2\pi}\int_{\varphi=0}^{\pi}\left(\begin{array}{c}\left\{3\Sigma^2\dfrac{(1-\sigma_{\theta\varphi,m}/\sigma_u)^2}{(1-\tau_{\theta\varphi,m}/\tau_u)^2} - 4\right\}\tau_{\theta\varphi}^2 \\[3mm] \left\{6 - 2\Sigma^2\dfrac{(1-\sigma_{\theta\varphi,m}/\sigma_u)^2}{(1-\tau_{\theta\varphi,m}/\tau_u)^2}\right\}\sigma_{\theta\varphi,m}^2\end{array}\right)\sin\varphi.d\varphi.d\theta} \qquad (34)$$

The equivalent stress histories are calculated using the stress tensor components in the critical region and the various criteria described above. The behavior of these stress histories is random and depends on the parameters of road roughness, vehicle velocity, and various maneuvers. Therefore, it is not possible to directly compare the stress histories. Nevertheless, the best technique to compare the equivalent stress histories is to study statistical parameters such as mean and deviation values. The mean and the deviation parameters are simultaneously shown in Figure 9 for different criteria by utilizing probabilistic distribution of stress.

The fatigue life of the component can be predicted qualitatively using this data. But, fatigue analysis should be performed to assess quantitatively the life of the automotive steering knuckle. As it is clear from the Fig. 9, the mean and the deviation values are similar for some criteria (e.g, Dang Van, Shariyat, Liu-Zenner, Energy approach, and Modified MacDiarmid). Hence, it is expected to be similar the life of knuckle using these criteria.

Fatigue life of steering knuckle has been estimated by utilizing rain-flow cycle counting technique (Nieslony Matlab Coding [33]) and Palmgren-Miner damage accumulation law. Fatigue life assessment algorithm used in the present research is summarized in Fig. 10 and the obtained fatigue lives of steering knuckle regarding the original Toe and Camber angles are reported in Table 4.

The lowest fatigue life has been predicted by using Liu-Zenner criterion for automotive steering knuckle made of ductile cast iron. In the other words, this criterion is more cautious than other criteria in this case.

Table 4
Fatigue life of steering knuckle under multi-axial non-proportional loadings caused by maneuvers on proving ground.

Type of the equivalent fatigue stress	Fatigue life (million cycles)
Von Misses	5.0074
Findley	4.1818
Dang Van	3.8945
MacDiarmid	4.114
Carpinteri-Spagnoli	4.3176
Shariyat	3.4206
Liu-Zenner	3.2179
Energy Approach by Shariyat	3.8289
Modified Findley	4.0462
Modified MacDiarmid	3.9698

4. Results

Fatigue analysis for each wheel angle was conducted according to the data in Tables 2 and 3. To compare the results, the main model was considered as proposed by the car manufacturer (the Toe angle is 0.1 and the Camber angle is +2). The results of fatigue life predicted for the main model are reported in Table 4. In this section, the results of all cases of Camber and Toe angles are shown in Figs. 11 and 12, respectively.
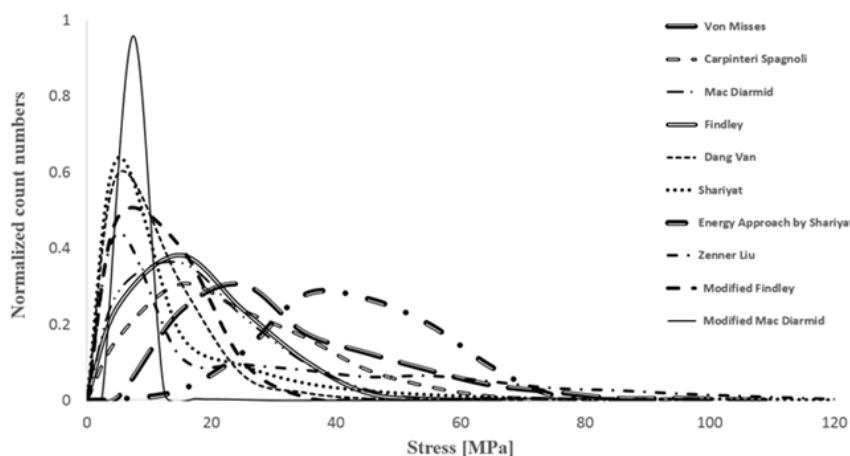
Fig. 9. Probabilistic distribution of equivalent stress by utilizing various criteria.
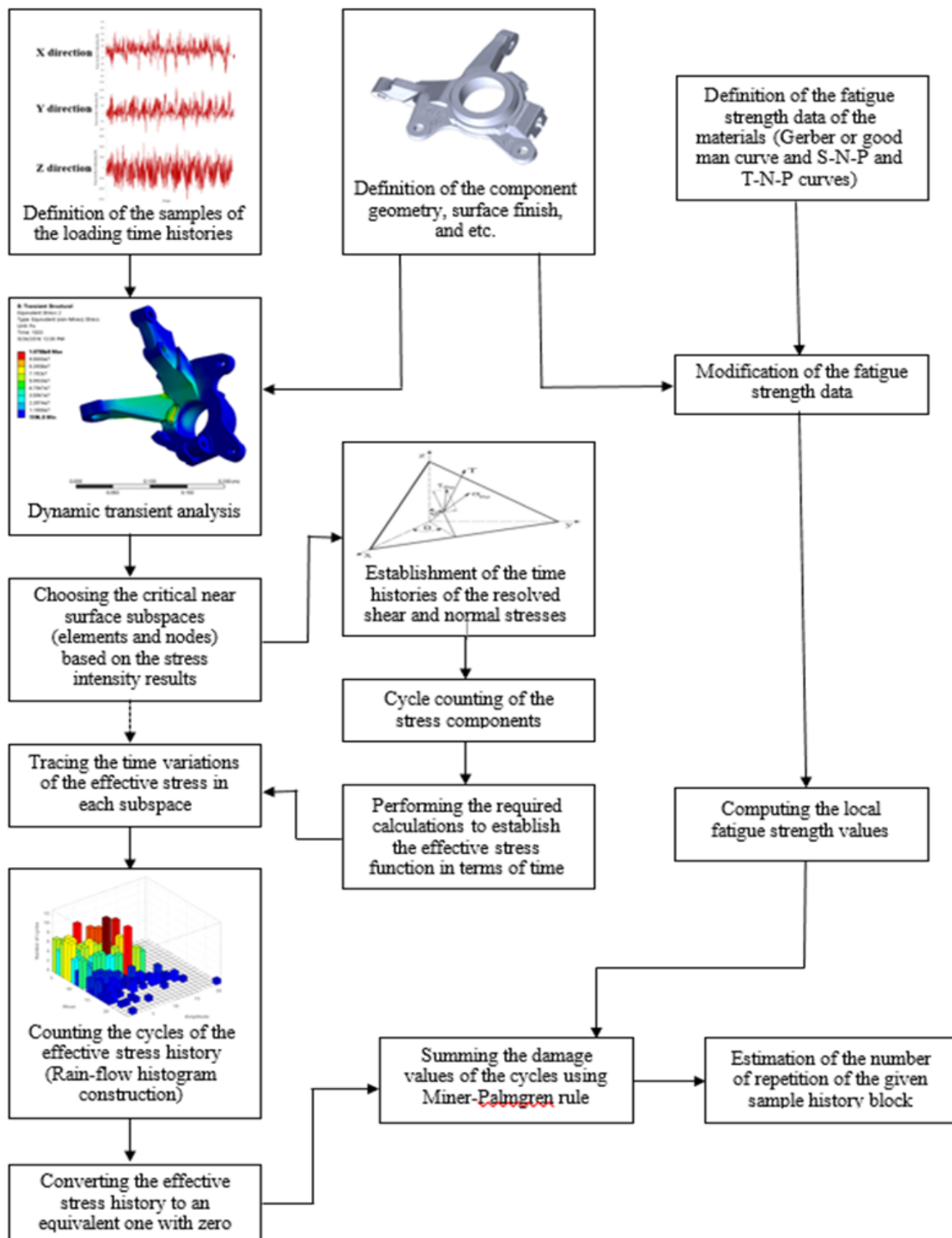
Fig. 10. Fatigue life assessment algorithm used in the present research.

According to the results obtained by utilizing the fatigue life assessment algorithm mentioned in section 3, visualized in Fig. 11, the fatigue lives of steering knuckle based on all considered criteria are greater when a bigger value of Camber angle is used. An average increase of 12% was found for fatigue life of the component when using a Camber angle equal to +2 instead of a positive value of 1 degree. Likewise, the minimum fatigue lives of the steering knuckle are related to Camber angle equal to -2 degrees. As is shown in Fig. 12, it is not possible to express a particular pattern for the fatigue life of steering knuckle vs. the Toe angle. But, most of the fatigue criteria predicted that a negative Toe angle of 0.2 degrees leads to the longest fatigue life of the component.
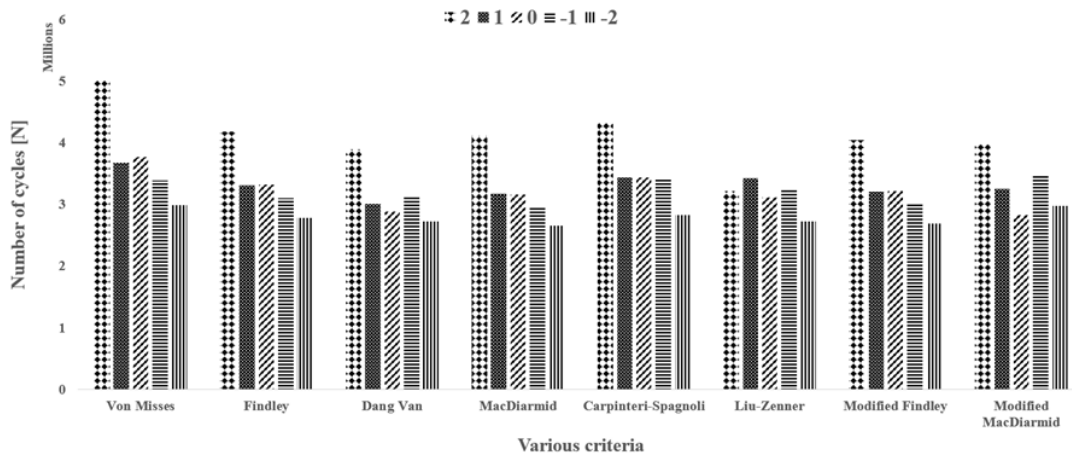
Fig. 11. Fatigue life of steering knuckle for several different Camber angles.
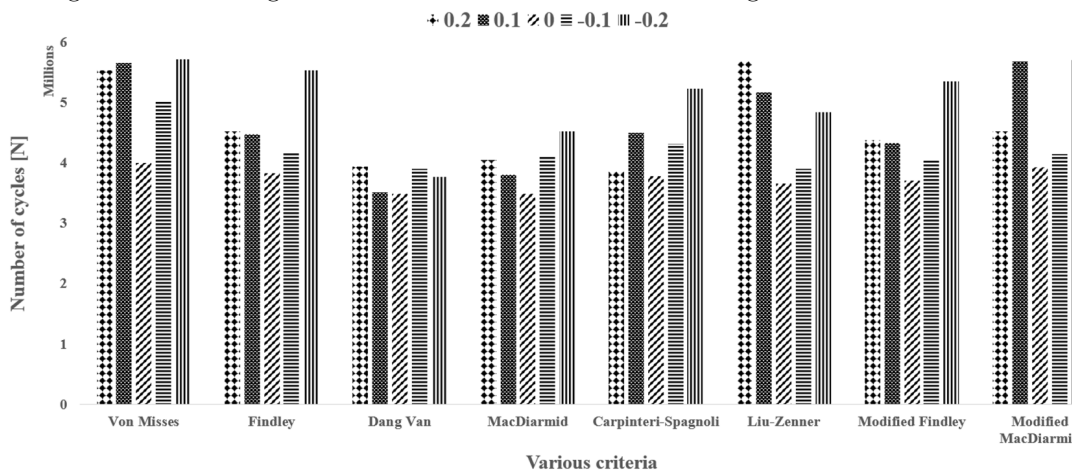
Fig. 12. Fatigue life of steering knuckle for several different Toe angles.

5. Conclusions

In the present research, the effect of wheel alignment on the fatigue life of automotive steering knuckle (a super critical component with a complicated geometry under multi-point 3D random inputs) was studied. In order to predict fatigue life of the component, the vehicle driving simulation was utilized. The equivalent road has developed as a combination of some rough events based on statistical data collected from different cities. The various actual load histories obtained through multi-body dynamics analysis of a full vehicle model were applied on connecting joints of the component. Finally, the fatigue lives of steering knuckle related to the different values of Toe and Camber angles were predicted by using the fatigue life assessment algorithm mentioned in section 3. The following conclusions can be drawn from this study:

1. The joint of the knuckle and the steering linkage is reported as the most critical region and the maximum value of Von-Misses stress in the critical area was estimated about 108MPa.

2. The lowest fatigue life has been predicted by using Liu-Zenner criterion for automotive steering knuckle made of ductile cast iron with original wheel angles. In the other words, this criterion is more cautious than other criteria in this case.

3. The maximum and minimum fatigue lives of the steering knuckle are related to Camber angles equal to +2 and -2 degrees, respectively. Furthermore, the results illustrated that the fatigue life of knuckle decreases by reducing the value of Camber angle. Specifically, it was indicated that the Camber angle suggested by the vehicle manufacturer is the most appropriate mode.

4. An average increase of 12% was found for fatigue life of component when using a Camber angle equal to +2 instead of a positive value of 1 degree.

5. Nevertheless, choosing the value of Toe angle as recommended by the manufacturer is not adequate. This study proposes that the value of Toe angle be equal to a negative value of 0.2 degrees in order to increase the fatigue life of steering knuckle. Needless to say, this suggestion should be studied with respect to car design issues such as sustainability, handling, and so on.

6. To have a safe car, it is necessary to periodically review the wheel angles of the vehicle and adjust them appropriately.

References

[1] M.W. Sayers, T.D. Gillespie, C.A.V. Queiroz, The International Road Roughness Experiment, The International Bank for Reconstruction and development, Washington, (1986).

[2] M.W. Sayers, T.D. Gillespie, W.D.O. Paterson, Guidelines for Conducting and Calibrating Road Roughness Measurements, The International Bank for Reconstruction and Development, Washington, (1986).

[3] M.W. Sayers, S.M. Karamihas, Interpretation of Road Roughness Profile Data, Prepared for Federal Highway Administration Contract DTFH 61-92-C00143, (1996).

[4] A. Gonzalez, E.J. Óbrien, Y. Li, K. Cashell, The use of vehicle acceleration measurements to estimate road roughness, Vehicle. Sys. Dyn., 46(6) (2008) 483-499.

[5] P. Johannesson, I. Rychlik, Modelling of road profiles using roughness indicators, Int. J. Veh. Des., 66 (2014) 317-346.

[6] P. Kumar, E. Angelats, An Automated Road Roughness Detection from Mobile Laser Scanning Data, The International Archives of Photogrammetry, Remote Sensing and Spatial Information Sciences, ISPRS Hannover Workshop, Hannover, Germany, 6-9 June (2017).

[7] R. Kumar, A. Mukherjee, V.P. Singh, Community sensor network for monitoring road roughness using smartphones, J. Comput. Civil. Eng., 31(3) (2017) 04016059-1-110.

[8] M. Choi, M. Kim, G. Kim, S. Kim, S.C. Park, S. Lee, 3D scanning technique for obtaining road surface and its applications, Int. J. Pr. Eng. Manuf., 18(3) (2017) 367-373.

[9] K. Reza Kashyzadeh, M.J. Ostad-Ahmad-Ghorabi, A. Arghavan, Study effects of vehicle velocity on a road surface roughness simulation, Appl. Mech. Mater., 372 (2013) 650-656.

[10] R.S. Barbosa, Vehicle dynamic response due to pavement roughness, J. Braz. Soc. Mech. Sci. Eng., 30(3) (2011) 302-307.

[11] B. GoenagaSilvera, L.G. Fuentes, O. Mora, Effect of Road Roughness and Vehicle Speed on Dynamic Load Prediction and Pavement Performance Reduction, Transportation Research Board 96th Annual Meeting, Washington DC, United States, 8-12 January (2017).

[12] G. Alessandroni, A. Carini, E. Lattanzi, V. Freschi, A. Bogliolo, A Study on the Influence of Speed on Road Roughness Sensing: The Smart Road Sense Case, Sens., 17(2) (2017) 305-325.

[13] G. Triantafyllidis, A. Antonopoulos, A. Spiliotis, S. Fedonos, D. Repanis, Fracture characteristics of fatigue failure of a vehicle's ductile iron steering knuckle, J. Fail. Anal. Prev., 9(4) (2009) 323-328.

[14] V. Sivananth, S. Vijayarangan, Fatigue life analysis and optimization of a passenger car steering knuckle under operating conditions, Int. J. Auto. Mech. Eng., 11(1) (2015) 2417-2429.

[15] E. Azrulhisham, Y. Asri, A. Dzuraidah, N. Abdullah, C. Hassan, A. Shahrom, Evaluation of fatigue life reliability of steering knuckle using Pearson parametric distribution model, Int. J. Qual. Stat. Reliab., 2010 (2010) 1-8.

[16] R. Vivekananda, A.V. Mythra Varun, Finite element analysis and optimization of the design of steering knuckle, Int. J. Eng. Res., 4(1) (2016) 121-135.

[17] K.S. Bhokare, G.M. Kakandikar, S.S. Kulkarni, Predicting the fatigue of steering knuckle arm of a sport utility vehicle while developing analytical techniques using CAE, Int. J. Sci. Res. Manag. Std., 1(11) (2013) 372-381.

[18] G.H. Farrahi, A. Khalaj, Estimation of fatigue damage caused by actual roads and maneuvers on proving ground, J. Achiev. Mater. Manuf. Eng., 14(1-2) (2006) 90-96.

[19] M. Shariyat, A fatigue model developed by modification of Gough's theory, for random non-proportional loading conditions and three-dimensional stress fields, Int. J. Fatigue., 30(7) (2008) 1248-1258.

[20] M. Shariyat, Three energy-based multiaxial HCF criteria for fatigue life determination in components under random non-proportional stress fields, Fatigue. Fract. Eng. Mater. Struct., 32(10) (2009) 785-808.

[21] M. Shariyat, New multiaxial HCF criteria based on instantaneous fatigue damage tracing in components with complicated geometries and random non-proportional loading conditions, Int. J. Damage Mech., 19(6) (2009) 659-690.

[22] M. Zoroufi, A. Fatemi, Durability Comparison and Life Predictions of Competing Manufacturing Processes: An Experimental Study of Steering Knuckle,the 25th Forging Industry Technical Conference, Detroit, (2004).

[23] A. Fatemi, M. Zoroufi, Fatigue Performance Evaluation of Forged versus Competing Manufacturing Process Technologies: A Comparative Analytical and Experimental Study, American Iron and Steel Institute, Toledo, (2004).

[24] M. Zoroufi, A. Fatemi, Experimental durability assessment and life prediction of vehicle suspension components: a case study of steering knuckles, Proc. Inst. Mech. Eng. D J. Automob. Eng., 220(11) (2006) 1565-1579.

[25] C.G.E. Schon, C.M. Angelo, F.A.C.E. Machado, The role of tire size over the fatigue damage accumulation in vehicle bodies, 20th European Conference on Fracture, Procedia Mater. Sci., 3 (2014) 331-336.

[26] C.M. Angelo, F.A.C.E. Machado, C.G.E. Schon, Influence of tire sizes over automobile body spectrum loads and fatigue damage accumulation, Mater. Des., 67 (2015) 385-389.

[27] J.Y. Wong, Theory of ground vehicle book, Third Edition, University of Ottawa, Wiley Interscience (2001).

[28] J. Marzbanrad, A. Hoseinpour, Structural optimization of MacPherson control arm under fatigue loading, Teh. Vjesn., 24(3) (2017) 917-924.

[29] D. Socie, G. Marquis, Multiaxial Fatigue, 1st Edition, USA: Society of Automotive Engineers SAE International, (2000).

[30] A. Carpinteri, A. Spagnoli, S. Vantadori, Multiaxial fatigue assessment using a simplified critical plane-based criterion, Int. J. Fatigue., 33(8) (2011) 969-976.

[31] A. Carpinteri, C. Ronchei, D. Scorza, S. Vantadori, Critical plane orientation influence on multiaxial high-cycle fatigue assessment, Phys. Mesomech., 18(4) (2015) 348-354.

[32] M. Shariyat, Automotive Body: Design and Analysis, First Edition, K.N. Toosi University Press, Iran, (2006).

[33] A. Nieslony, Determination of fragments of multiaxial service loading strongly influencing the fatigue of machine components, Mech. Sys. Sig. Proc., 23(8) (2009) 2712-2721.